

Blueprint of optically addressable molecular network for quantum circuit architecture

Jiawei Chang^{1,2,3&}, Tianhong Huang^{1,2,3&}, Lin Ma^{1,2,3}, Taoyu Zou^{4,*}, Wei Wu^{5,†} and Hai Wang^{1,2‡}

¹*Yunnan Key Laboratory of Metal-Organic Molecular Materials and Devices Kunming University Kunming Yunnan Province P. R. China*

²*Key Laboratory of Yunnan Provincial Higher Education Institutions for Organic Optoelectronic Materials and Devices, Kunming University, Kunming, Yunnan Province, P. R. China*

³*School of Physical Science and Technology, Kunming University, Kunming, Yunnan Province, P. R. China*

⁴*Yunnan Ocean Organic Optoelectronic Technology Ltd, Kunming, 650214, Yunnan Province, P. R. China and*

⁵*UCL Institute for Materials Discovery, University College London, Gower Street, London WC1E 6BT, United Kingdom*

(Dated: September 13, 2022)

Organic molecules could be ideal platform for quantum computation. To build a quantum circuit, we need to have the optimal control on both the quantum bit (qubit) and the quantum gate operations. Here we compute the exchange interaction between organic radical (qubit) and optically induced triplet (spin coupler), and spin dynamics simulations with a realistic open quantum system setup. Our calculations suggest a much-enhanced exchange interaction and entangled radical spins due to mediating triplet, which implies the great potential of using molecules for quantum computation. Our calculations are also in a good agreement with the previous experimental and simulation works, thus laying a solid foundation for our proposal - a quantum processor blueprint that relies on molecular network and programable optical nano-device for the realisation of quantum circuits. This work will open up a new direction to explore the 2D molecular networks for the quantum information processing at high temperature.

I. INTRODUCTION

The theoretical design of quantum computing (QC) system is important to address the main challenges in QC – a good *control* on the interaction among *well-isolated* quantum bit (qubit) at a realistic working condition such as room temperature. In the so-called ‘quantum computing stack’ (QCS) [1], the quality of the qubit technology is the key foundation for building a quantum computer. On top of this, the control engineering requires accurate manipulations of quantum gates, for which we might be able to take advantages from the well developed technologies, such as electron spin resonance and optical stimulation and detection. The qubit technology and control engineering form an indispensable basis for quantum software and algorithms in the upper levels in QCS. Recent developments in QC [2–5], based on superconducting circuits, have demonstrated the superior capacity of the quantum computer in dealing with some particular problems that are inconvenient for the classical counterparts. Although small QC systems have been fabricated [3, 4, 6, 7], we are still facing many challenges, especially in (i) the realisation of room-temperature quantum gate operations and (ii) the further elevation of the number of the integrated qubits with quantum error corrections [1]. These two concerns have stimulated the proposals of novel QC platforms recently, which exploited

the advantages of the spin qubit and optically accessible triplet state in organic molecules [8]. More strikingly, recent experimental work on molecular quantum qubits has shown that their promise for QC [9, 10], in which the spin initialisation, readout, and coherence have been demonstrated. In addition, recently the studies of two-dimensional magnetic materials have been surging rapidly [11], which have a good potential for quantum computing architecture design. Hence, based on the previous work [8, 9], two-dimensional organic molecular networks (2D OMNs), which can be chemically synthesised and manipulated, have a great potential in overcoming the challenges aforementioned owing to the long coherence time at high or even room temperature [12–15] and the ease of QC network structuring. Many mature QC techniques such as single qubit initialisation and readout are readily transferable to OMN. The energy efficiency and footprints of QC have just been noticed, which is an important aspect for developing quantum information science without worsening the Greenhouse effect [16]. To this end, high-temperature (or even room-temperature) QC has a clear advantage over those QC designs relying on the extremely low-temperature environment.

Organic radicals, containing $\frac{1}{2}$ -spins, are a natural realisation of a qubit [17]. An example for the organic radical, 4,4,5,5-tetramethyl-1-yloxyimidazolin-2-yl (TYY), is shown in Fig. 1a. The spin relaxation and coherence times of organic radicals can be very long (up to seconds) due to small spin-orbit coupling and weak hyperfine interactions [14, 18]. For multi-qubit gate operations, a promising route to control the interaction between radicals is optical excitation [9], which can circumvent additional electrodes that will induce significant decoherence [19]. Recently electro-optical transducer has been used

*Electronic address: taoyuzou@sina.com

†Electronic address: wei.wu@ucl.ac.uk

‡Electronic address: wang_lab@sina.com

& These authors contributed equally to this work.

to detect the quantum state optically to read out the quantum bit [20]. The promising molecular candidate for demonstrating optically controlled quantum gate operations would ideally consist of two or more radicals linked by the optically active spin coupler. For example, di-phenyl anthracene (DPA) molecule, shown in Fig.1b, can be excited from a singlet ground state to a triplet state due to the inter-system crossing (ISC) [21, 23], thus mediating the interaction between radicals. By linking the radicals and spin couplers, we can form a multi-radical-triplet system (MRTS), such as the biTTY-DPA, as shown in Fig.1c. The radicals are typically sufficiently far apart that the exchange interaction between them is negligible when the coupler is in its ground state, but the coupling is turned on while the triplet persists. Organic chemical synthesis provides us with a vast database for the choice of radicals and spin couplers [12]. The spin coupling mechanism is shown in Fig.1d. The lifetime of the triplet, characterized by the decay parameter k_{tg} , is usually long (ms) because the decay to the singlet ground state is forbidden due to spin momentum conservation and hence dominated by non-radiative processes. Extensive experimental efforts, combining time-resolved electron paramagnetic resonance (TREPR) and optical excitations [21, 22, 24–28] have been made to control exchange interactions in MRTS. There have been a number of previous studies for this type of system, which have demonstrated the transient exchange interaction between the radicals and the triplet [26, 27]. It has also been shown that the radical spins may be controlled by optical excitation [26]. This spin coupling mechanism offers a promising route to control quantum gate operations at a time scale of $\sim ns$. The fabrications of such OMNs have been demonstrated experimentally in the previous work [29, 30]. Most of the TREPR experiments can be performed at the high temperature (77 K, the boiling point of liquid nitrogen), which can bring forward the advantages in developing more practical quantum technologies. The observation of spin dynamics and coherence, important for quantum gate operations, can be carried out by using TREPR [12, 14]. The realization of spin qubits and their control would therefore be less challenging than the nitrogen-vacancy centres and silicon impurities, but slightly more difficult than the superconducting qubits, in terms of experimental conditions required. Moreover, the 2D OMNs have been developed substantially recently [29, 30], which can be used as the material basis for quantum circuit architectures [3], thus leading to much higher number of qubits and high-temperature quantum gate operations. We not only take advantages from the recent development of the programable photonic quantum circuits, but also integrate spin qubits with photonics, thus realising high-temperature QC.

Previously, a first-principles calculation was carried out for the spin-2 state of the biTTY-DPA molecule [27] and a qualitative model for the spin dynamics in MRTS has been proposed [31]. To the authors' best knowledge, such optically induced exchange couplings and simula-

tions of spin dynamics have not been addressed quantitatively previously. Moreover, there have been few reports for (i) the quantitative calculation of the exchange interaction between the transient triplet and radicals in MRTS and (ii) the simulation of the TREPR spectra using the theory of open quantum systems [32], which are the focus of this work. Our calculations of the exchange interactions are in a good agreement with the previous experimental results, with a general method for computing exchange interactions in MRTS proposed. Our simulations of TREPR spectra are also in a qualitative agreement with the previous experiments [27]. Moreover, we have further proposed a molecular architecture in combination with appropriate optical nano-devices to scale up the quantum circuits, thus paving the way for tackling the challenges aforementioned.

II. COMPUTATIONAL DETAILS

A. First-principles density-functional-theory calculations for exchange interactions

The first-principles calculations have been carried out using hybrid exchange density function theory (HDFT) with a 6–31G basis set in the Gaussian 09 code [33]. The self-consistent field (SCF) procedure was converged to a tolerance of 10^{-6} a.u. (~ 0.3 Kelvin). The broken-symmetry method [34] was used to allow spins to localize on the radicals and the convergence to a low-spin configuration. Electronic exchange and correlation are described using the B3LYP hybrid exchange density functional [35], the advantages of which include a partial elimination of the electronic self-interaction error and thus a balance of the tendencies to delocalize and localize one-electron wave-functions. The B3LYP density functional has previously been shown to provide an accurate description of the electronic structure and magnetic properties for both inorganic and organic compounds [36, 37].

Supposing that an MRTS consists of two radicals and one spin coupler, and that the exchange interaction dominates over both dipolar interactions and spin-orbit coupling, then the Heisenberg spin Hamiltonian before optical excitations reads

$$\hat{H}_0 = J_0 \hat{s}_1 \cdot \hat{s}_2, \quad (1)$$

where J_0 is the exchange interaction between radical spins \hat{s}_1 and \hat{s}_2 , which can be computed as the energy difference between the triplet and broken-symmetry (BS) states of radicals, $J_0 = 2(E_{\text{triplet}} - E_{\text{BS}})$. When the spin coupler is in a triplet state after optical excitations, the spin Hamiltonian changes to

$$\hat{H}_1 = J_1 \hat{s}_1 \cdot \hat{S} + J_2 \hat{S} \cdot \hat{s}_2 + J_3 \hat{s}_1 \cdot \hat{s}_2, \quad (2)$$

where J_1 (J_2) is defined as the exchange interaction between radical spins \hat{s}_1 (\hat{s}_2) and the triplet spin \hat{S} . J_3 is

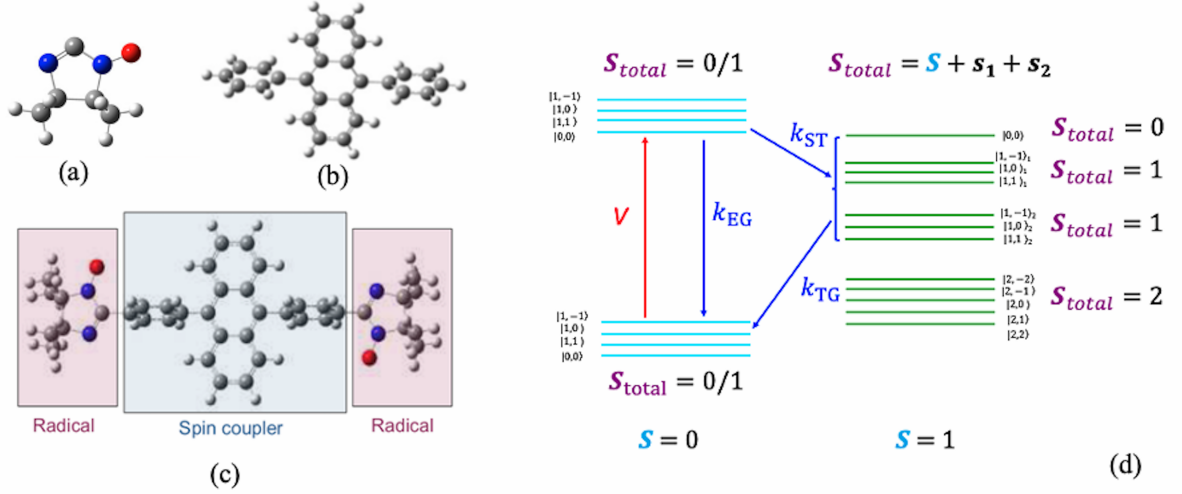


FIG. 1: (Color online.) One example for the MRTS systems and the spin coupling mechanism are shown. (a) TYY radical, (b) DPA spin coupler, and (c) combined double-radical triplet system. In (d), we have shown the coherent and incoherent processes. The coherent processes include spin-spin interaction among radicals and triplet and optical driving field (V), while the incoherent one the inter-system crossing and the decays of the triplet and singlet excited states. The decay rates k_{ST} , k_{TG} , and k_{EG} are also illustrated.

the exchange interaction between two radical spins after optical excitations. To compute J_1 , J_2 , and J_3 , we first find the total energies of the states $|a\rangle = |\uparrow\uparrow\uparrow\rangle$, $|b\rangle = |\uparrow\uparrow\downarrow\rangle$, $|c\rangle = |\downarrow\downarrow\downarrow\rangle$, and $|d\rangle = |\downarrow\uparrow\uparrow\rangle$, where $\uparrow(\downarrow)$ is defined as the spin state $|s = \frac{1}{2}, s_z = \frac{1}{2}\rangle$ ($|s = \frac{1}{2}, s_z = -\frac{1}{2}\rangle$) of a radical and \uparrow as $|S = 1, S_z = 1\rangle$ for the spin-coupler triplet. Then we can have

$$\begin{aligned} J_1 &= (\Delta E_{ac} + \Delta E_{bd})/2, \\ J_2 &= (\Delta E_{ac} - \Delta E_{bd})/2, \\ J_3 &= \Delta E_{cd} + \Delta E_{ab}, \end{aligned} \quad (3)$$

where $\Delta E_{ij} = E_i - E_j$ is defined as the energy difference between the states with the spin configurations i and j ($\in \{a, b, c, d\}$).

Note that the broken-symmetry singlet and triplet states formed by two radical spins alone have the same z -component of spin as $|c\rangle$ and $|b\rangle, |d\rangle$, respectively, but much lower energies, owing to the triplet excitation energy (\sim eV in general). The Kohn-Sham orbitals therefore need to be repopulated in order to drive the system into $|b\rangle$, $|c\rangle$, or $|d\rangle$. If two radicals are symmetric, then $E_b = E_d$ and therefore

$$\begin{aligned} J_1 &= J_2 = \Delta E_{ac}/2, \\ J_3 &= \Delta E_{cb} + \Delta E_{ab}. \end{aligned} \quad (4)$$

The expectation value of the total spin operator $\hat{S}_{total} =$

$\hat{s}_1 + \hat{s}_2 + \hat{s}_3$ is 6 for the state $|a\rangle$ (since it is a total spin eigenstate with $S_{total} = 2$), 3 for $|b\rangle$ and $|d\rangle$, and 2 for $|c\rangle$. We adopted that the exchange interactions are antiferromagnetic (AFM) when $J > 0$ while ferromagnetic (FM) when $J < 0$. The spin Hamiltonians in eq.1 and eq.2 and the computation of the exchange interactions therein can be easily generalized to the molecular structure with more radicals.

Here J_1 is equal to J_2 because the biTYY-DPA molecule has an inversion symmetry. J_0 , J_1 and J_3 were computed for the dihedral angles between the phenyl ring and the anthracene, ranging from 0° (coplanar) to 90° (perpendicular) with 10° increments. In all the calculations, we froze the TYY radicals and rotate only the phenyl ring, which meant we assumed the dihedral angles at each end of the coupler are equal.

B. The time evolution of the density matrix and TR-EPR spectra simulations

1. System Hamiltonian

After taking into account the optical driving field, our total Hamiltonian reads

$$\begin{aligned}
\hat{H}_{opt} = & |S_0\rangle[\hat{H}_0 + g_r\mu_B\vec{B} \cdot (\vec{s}_1 + \vec{s}_2)]\langle S_0| + \\
& |S_1\rangle[\hat{H}_0 + g_r\mu_B\vec{B} \cdot (\vec{s}_1 + \vec{s}_2)]\langle S_1| + \\
& |T_1\rangle[\hat{H}_1 + g_r\mu_B\vec{B} \cdot (\vec{s}_1 + \vec{s}_2) + g_c\mu_B\vec{B} \cdot \vec{S} + D\hat{S}_z^2 + E(\hat{S}_x^2 - \hat{S}_y^2)]\langle T_1| + \\
& V(|S_0\rangle\langle S_1| + |S_1\rangle\langle S_0|).
\end{aligned} \tag{5}$$

Here S_0 is the singlet ground state, S_1 the first singlet excited state, and T_1 the triplet ground state. D and E are the zero-field splittings (ZFS) for the triplet. g_r is the g-factor for the radical spin, while g_c for the coupler spin. Here V is the transition matrix element between the ground and excited singlet states (S_0 and S_1) due to the optical driving field. \vec{B} is a static magnetic field and μ_B is the Bohr magneton. \hat{H}_0 and \hat{H}_1 are defined in eq.1 and 2, respectively. Here we assume that the exchange interaction between radicals J_0 is unchanged in the singlet excited states.

2. Quantum jump operators due to the system-environment couplings

To include the environment effects on the time evolution of the density matrix, we used the super operators (the Liouvillian) within the Markovian approximation, leading to the Lindblad formalism. These super operators read

$$\hat{L}_i\hat{\rho} = \sum_{\mu=1}^{n_i} \gamma_i^\mu [\hat{l}_i^\mu \hat{\rho} \hat{l}_i^{\mu\dagger} - \frac{1}{2}\{\hat{\rho}, \hat{l}_i^{\mu\dagger}\hat{l}_i^\mu\}] \tag{6}$$

Here $\hat{\rho}$ is the density matrix for MRTS. The incoherent processes are described by γ_i^μ (the decoherence rate) and \hat{l}_i^μ (the quantum jump operator), where i labels different decoherence processes and μ the operators in the process. And n_i is the number of the operators in each physical process i . For our system, $i = 1$ to 5. $\hat{L}_{1,2}$ with $n_{1,2} = 3$ is used to describe the relaxation of the radical spins \vec{s}_1 and \vec{s}_2 as follows, $\hat{l}_1^{1,2} = \hat{s}_{1,2}^-$ (spin- $\frac{1}{2}$ lowering operator), $\hat{l}_2^{1,2} = \hat{s}_{1,2}^+$ (spin- $\frac{1}{2}$ raising operator), and $\hat{l}_3^{1,2} = \hat{s}_{1,2}^z$ (the z -component of the spin- $\frac{1}{2}$). The \hat{s}^z operator is responsible for the pure dephasing of quantum states, whereas \hat{s}^+ and \hat{s}^- for quantum jumps. \hat{L}_2 with $n_2 = 8$ is used as a super operator to describe the relaxation of the triplet state. We have used the corresponding eight Gell-Mann matrices for these operators. Moreover, we have taken into account the spin-spin (transverse spin) relaxation [38] within the mean-field approximation induced by the interaction between the spins in the system and those in the environment, i.e., $\hat{s}_1\hat{s}_2 \sim \langle \hat{s} \rangle_1 \hat{s}_2$. Hence the T_2 relaxation processes can be absorbed into the Lindblad formalisms $\hat{L}_{1,2}$ described above.

Here, we have taken into account the ISC in \hat{L}_3 , assuming that the total spin angular momentum and its z -component are both conserved, i.e., $S_{\text{total}} = 0$ or 1 (twice), thus obtaining the following operators. \hat{L}_3 with $n_3 = 7$ describes the transitions from the single excited state to the triplet state. For example, some of the operators read $\hat{l}_3^1 = |0,0\rangle_{T_1}\langle 0,0|_{S_1}$ and $\hat{l}_3^2 = |1,-1\rangle_{T_1}\langle 1,-1|_{S_1}$. Here we use $|S_{\text{total}}, S_{\text{total},z}\rangle$ to represent our states formed in the triplet (T_1) and the S_1 manifolds as shown in Fig.1(d). Similarly we can define the decay operator \hat{L}_4 ($n_4 = 7$) for the transition from the triplet state to the singlet ground state. For example, some of the operators read $\hat{l}_4^1 = |0,0\rangle_{S_0}\langle 0,0|_T$ and $\hat{l}_4^2 = |1,-1\rangle_{S_0}\langle 1,-1|_T$. The fifth super-operator \hat{L}_5 is responsible for the spontaneous decay of the singlet excited state (S_1) down to the ground state (S_0). There are four operators ($n_5 = 4$), including $\hat{l}_5^1 = |0,0\rangle_{S_0}\langle 0,0|_{S_1}$, $\hat{l}_5^2 = |1,-1\rangle_{S_0}\langle 1,-1|_{S_1}$, $\hat{l}_5^3 = |1,0\rangle_{S_0}\langle 1,0|_{S_1}$, and $\hat{l}_5^4 = |1,1\rangle_{S_0}\langle 1,1|_{S_1}$. All the coupling parameters γ_i^μ (i from 1 to 5) have been simplified by using a single parameter γ_{radical} , γ_{triplet} , k_{st} , k_{tg} , and k_{eg} for these five incoherent processes.

3. The total Liouvillian and the simulation of TREPR spectra

Therefore the total Liouvillian operator can be written as follows.

$$\frac{d\hat{\rho}}{dt} = \hat{\mathcal{L}}\hat{\rho} = -i[\hat{H}_{opt}, \hat{\rho}] + [\sum_{i=1}^5 \hat{L}_i]\hat{\rho} \tag{7}$$

Here the first part is the coherent interaction from the effective spin Hamiltonian and optical field (see eq.5), which is the commutator between the Hamiltonian and the density matrix. The second part includes the incoherent processes associated with relaxations and crossovers between states (see eq.6). Therefore, we have 20 by 20 Hamiltonian matrix (4 for the singlet ground and excited states with radicals, 12 for the triplet ground states with radicals), leading to a 400 by 400 Liouvillian.

The TR-EPR spectra can be computed as follows [39, 40],

$$I(t, \omega) = |\text{Tr}\{\hat{\rho}(t)S_x^{\text{total}}[i\hat{\mathcal{L}} - \omega I]^{-1}S_x^{\text{total}}\}|. \tag{8}$$

Here S_x^{total} is the x -component of the total spin and ω is the microwave field frequency.

III. RESULTS AND DISCUSSION

A. DFT calculations for exchange interactions

When the spin coupler is in its ground state, the two TYY radicals interact weakly through the spin polarisation (induced by the radical spin) on the coupler. However, after the optical excitation and ISC, the spin polarisation on the coupler is mostly dominated by the triplet spin, as shown in Fig.2(a-f). In our calculations, J_3 is three to four orders smaller than J_0 for all the dihedral angles studied (Fig.2g). We therefore neglect J_3 in what follows. When the dihedral angle is 0° , J_0/k_B is predicted to be 16.8 K and J_1/k_B to be -461.4 K, which is above the room temperature. When the dihedral angle is 60° , which is a geometry that has been observed in the DPA crystal structure [41], J_0/k_B is predicted to be 15.2 K and J_1/k_B to be -22.8 K. When the dihedral angle is 90° , J_0 is computed to be negligible, however the dipolar interaction between the spins is estimated to be $\sim 10^{-4}$ K as the distance between radicals is ~ 17 Å, and J_1/k_B is predicted to be -2.0 K. These results are consistent with the TREPR experiments for the magnetic properties of biTYY-DPA, which confirms the radical spins are aligned after the optical excitation and ISC on DPA [26].

The computed J_1 is FM (favouring parallel spins) for all the dihedral angles whereas J_0 is AFM (favouring antiparallel spins) or negligible. It is clear that at suitable temperatures the optical excitation and ISC can change the spin alignment of the radicals from AFM to FM. This implies that biTYY-DPA can not only work as an optically controlled single-molecule magnetic switch, but also has the potential for quantum gate operations as the magnitude of the exchange interaction increases significantly. This can potentially work at room temperature if the molecule can be prepared with a dihedral angle smaller than 20° on a surface, as suggested in Fig.2g. The calculated spin densities help to reveal the nature of the exchange interactions between the radicals and the triplet on DPA. The spin densities of the three spin configurations $|a\rangle$, $|b\rangle$, and $|c\rangle$ for the dihedral angle of 0° (90°) are shown in Fig. 2a-c (d-f). J_1 decreases as we enlarge the dihedral angle because the rotation of the phenyl ring away from the coplanar geometry suppresses the delocalisation of the π -orbitals of DPA, which dominate the wave function of the triplet exciton. This is manifested by the much smaller spin densities on phenyl rings with the dihedral angle equal to 90° than 0° , as shown in Fig. 2(a-f). In contrast to these large variations on the phenyl rings the spin densities on the radicals are insensitive to the dihedral angle: Mulliken population analysis yields a spin moment of $\sim 0.3\mu_B$ on the nitrogen and $\sim 0.5\mu_B$ on the oxygen for all the dihedral angles.

The mechanism for the strong radical-triplet exchange interaction J_1 can be understood using the Ovchinnikov's topological spin alternation rule for π -conjugated systems [26, 42, 43]: the spin-up and spin-down densities alternate on the neighbouring carbon atoms. The underlying physics of this rule is related to the formation of the spin polarisation induced by electron delocalisation in a π -conjugated system, similar to the indirect exchange mechanism in inorganic insulators [44] and the Lieb's theorem for the bipartite graphene lattice [43]. In the $|a\rangle$ state, the spin densities are consistent with the Ovchinnikov's topological spin alternation rule, whereas in the $|b\rangle$ and $|c\rangle$ states the rule is violated when the spin-up densities meet at the junction between the phenyl ring and the TYY radicals (highlighted by the red arrows in Fig.2b,c). Therefore, the spin-aligned state $|a\rangle$ is favoured and the exchange interaction for the triplet excited state on DPA is FM.

B. Spin dynamics with optical excitations and TREPR spectra simulations

We have also computed the dynamics of the whole system based on the theory of open quantum systems described in §II B. In Fig.3 (a), we show the time evolution of the off-diagonal term (coherence) for the reduced density matrix of the two radicals ($|\frac{1}{2}, \frac{1}{2}\rangle\langle\frac{1}{2}, -\frac{1}{2}|$), after tracing out the triplet manifold. We can see that the magnitude of the matrix element will increase when applying the optical driving field, and then will decay slowly as the triplet vanishes. This suggests the exchange interaction between radical and triplet induced by the optical field will trigger the coherence or entanglement between the two radical spins. We have also shown the diagonal term (population) for the $|\frac{1}{2}, 1, -\frac{1}{2}\rangle$ state in the density matrix, which shows the Rabi-oscillation characteristics, indicating the coherence created during this process. In Fig.3 (c), the tomography for the magnitudes of the reduced density-matrix of the two radicals at the early stage ($T = 6.2$ ps) of the time evolution after applying the optical excitation has been plotted, in which we can clearly see the nonzero off-diagonal term for spin coherence. Here $|1\rangle = |\frac{1}{2}, \frac{1}{2}\rangle_L |\frac{1}{2}, \frac{1}{2}\rangle_R$, $|2\rangle = |\frac{1}{2}, \frac{1}{2}\rangle_L |\frac{1}{2}, -\frac{1}{2}\rangle_R$, $|3\rangle = |\frac{1}{2}, -\frac{1}{2}\rangle_L |\frac{1}{2}, \frac{1}{2}\rangle_R$, and $|4\rangle = |\frac{1}{2}, -\frac{1}{2}\rangle_L |\frac{1}{2}, -\frac{1}{2}\rangle_R$ (L and R label the radical on the left and right, respectively). We have also investigated the TREPR spectra at the early stage ($T = 6.2$ ps) in Fig.3(d-f). We have used different parameters for the exchange interaction between radical and triplet, which are comparable to the range of the exchange interactions computed by DFT as shown in §III A. The exchange interaction between triplet and radical is -10 , -10^3 , and -10^5 mT for Fig.3(d), (e), and (f), respectively. For the static magnetic field (X-band), the spin anisotropy, spin relaxation rates, the ISC rate, and spontaneous decay rate, we have used the same parameters as the previous work [8] When the exchange interaction is smaller than the static magnetic

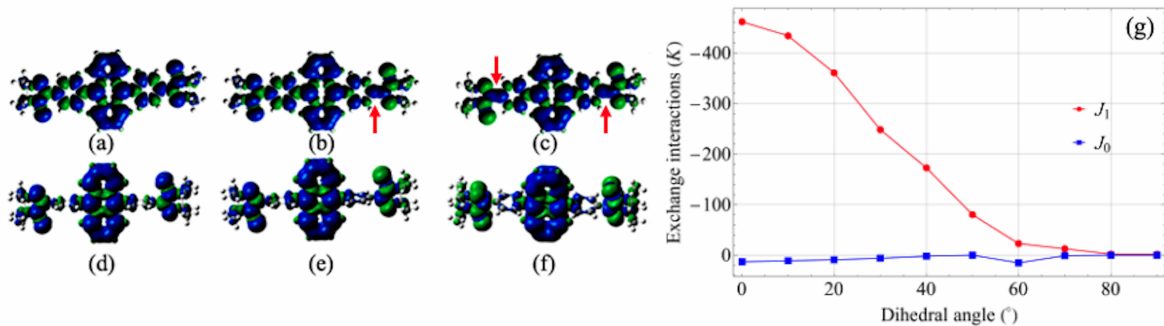


FIG. 2: (Color online.) The isosurfaces of spin densities in biTTY-DPA with the dihedral angle of 0° (90°) with spin configurations $|a\rangle$, $|b\rangle$, and $|c\rangle$ are shown in (a) - (c) ((d)-(f)). Positive is in blue and negative in green. The isosurface value is set to $0.01e/\text{\AA}^3$. In (g), the exchange interactions J_0 (blue squares) and J_1 (red circles) are plotted as functions of the dihedral angle between the anthracene and the phenyl ring. Notice that for all the angles studied here, the sign of the exchange interaction is switched by optical excitation and ISC, and that J_1 decreases as the dihedral angle increases owing to the suppression of the triplet wave function on DPA. On the other hand, the dependence of J_0 on the dihedral angle is more complicated because the exchange interaction between radicals is through spin polarisation.

field (~ 350 mT, X-band EPR), there are more features in the spectra than those from the much larger exchange interaction. The side peaks stem from the triplet state of DPA while the central peaks (when the exchange interaction is -10 mT) originate from the radical spins, which were renormalized by the interactions with the triplet on DPA. Our EPR simulations are also consistent with the experimental results in Ref.[26, 27], except that the authors therein distinguished the absorption and emission. The EPR spectra for the larger exchange interaction are saturated due to the limitation of the magnitude of the static magnetic field, which implies the EPR spectra will be dominated by the exchange interaction between the radicals and the triplet. Therefore, in this range of static magnetic field, we can only see the effect from the spin anisotropy (D and E). For the large exchange interaction, we need other instruments to probe them, such as neutron scattering[45].

C. Quantum computer-aided design based on molecules

Based on the first-principles calculations of the exchange interactions and the TR-EPR simulations for an open quantum molecular system for two radicals and one spin coupler, we can extend this to a quantum-circuit architecture as shown in Fig.4. The reason for doing this is that the dominant coupling mechanism is between radical pairs and the universal quantum gate can be realised by any of the non-trivial two-qubit gate operation in addition to one-qubit operation. Recently the quantum computer-aided design (QCAD) has been proposed for the quantum computing architectures based on silicon quantum dots [46–48], which has a huge potential to optimise the quantum circuit design, thus improving the design efficiency, although it is still in the early stage.

QCAD includes the modelling and design of the base material structures, a single qubit, and multiple qubits, in addition to the dynamics of the quantum states. Here we employed QCAD to design molecular networks in general and corresponding optical devices for control to realise the quantum computation. As shown in Fig.4, a two-dimensional molecular network consists of TYY radicals (qubits) and phthalocyanine (Pc, working as a spin coupler), which can be either chemically bonded by suitable bridging molecule structures or linked through Van der Waals forces. Here we have chose Pc as a spin coupler because (i) Pc has good optical properties [23] and (ii) as a planar molecule, Pc is great building block to form 2D OMN. On top of this molecular network, we can build in the optical devices that will control the spin and electronic states of the Pc molecules, i.e. inducing a transition from the singlet to the triplet, thus mediating the interactions among the radicals. The fabrication of the optical devices in such small length scale (a few nanometers) might be difficult, but the similar design has been demonstrated recently by using an optical tweezer [49]. Moreover, we can explore the triplet excited states, i.e., promoting the triplet from the ground state to the excited state, which is expected to allow us to further separate the radicals, ideally tens of nanometer distances, thus easing the design and fabrication of the optical devices. Regarding the feasibility of the fabrication optical devices, one choice is to use nanometer-size single photon emitter recently developed such as the gold tips or nanoscale gaps on WSe₂ [50–52]. In addition, the quantum calligraphy, in which encoding strains into the 2D materials can be used to create and locate the single-photon emitters with a precision of nanometers [53]. Also, the nanometer-sized single photon emitters can be fabricated by using quantum dots [54]. Another alternative for the optical devices is to use organic molecules such as Pc and dibenzoterrylene that has a

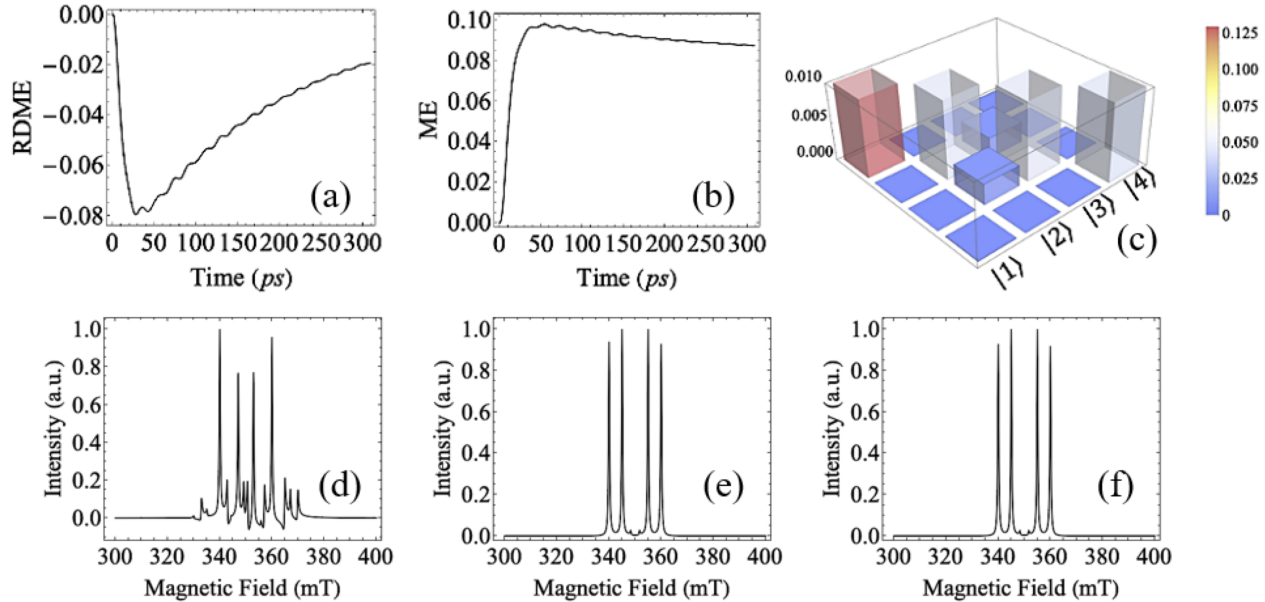


FIG. 3: (Color online.) The time evolutions of the density matrix elements are shown. In (a), we show the off-diagonal term ($|\frac{1}{2}, \frac{1}{2}\rangle\langle\frac{1}{2}, -\frac{1}{2}|$) of the reduced density matrix element for two radicals, which indicates the entanglement between two radicals created during this process. In (b), we show the populations for the state $|\frac{1}{2}, 1, -\frac{1}{2}\rangle$, which has a Rabi-oscillation behaviour. In (c), we have computed the magnitudes of the reduced density matrix for two radicals as a tomography. From (d)-(f), we show the EPR spectra with different exchange interactions between radical and triplet ($J_1 = -10, -10^3, -10^5$ mT)

very good optical emission properties [23, 55] and also is compatible with the spin couplers, thus further easing the integration with the molecular quantum computing network. As shown in the above sections, the mediating couplings and quantum dynamics have been calculated, which suggests this proposal is feasible. The persistence of the exchange interaction between the radical and the triplet could be problematic for read-out. Further work will therefore be required either to identify mechanisms that can turn off the interaction after a defined time in order to read out quantum information, or to understand how to exploit this always-on interaction to perform quantum computation [56]. Our design also involves much higher energy scales that would be a substantial advantage compared with the inorganic counterpart such as silicon quantum dots [47]. By programming the operations of the optical devices we can then control the interactions among radicals, thus realising quantum computing [3]. Our design could also facilitate the current development of quantum simulations, i.e., exploring quantum computing for computational chemistry. Here the molecular quantum computing architecture could be

explored to simulate quantum molecular systems.

IV. CONCLUSIONS

We have computed the exchange interaction between the radicals and optically induced triplets in biTTY-DPA from first principles, which are consistent with the previous experimental results observing the spin alignment with optical excitations. We find the radical-triplet exchange interactions J_1 are enhanced very significantly (by approximately two orders of magnitude on average) relative to the ground-state coupling J_0 between the radicals without optical excitations. This large ratio of J_1 to J_0 implies the possibility of 'switching on' a two-qubit interaction by optical excitation, thus facilitating the construction of molecular networks for quantum computing. The time evolution of the reduced density matrix for the radical suggests we could create the entanglement between the radicals through the optical excitation and ISC. We have also calculated the TREPR spectra, which is in agreement with the previous exper-

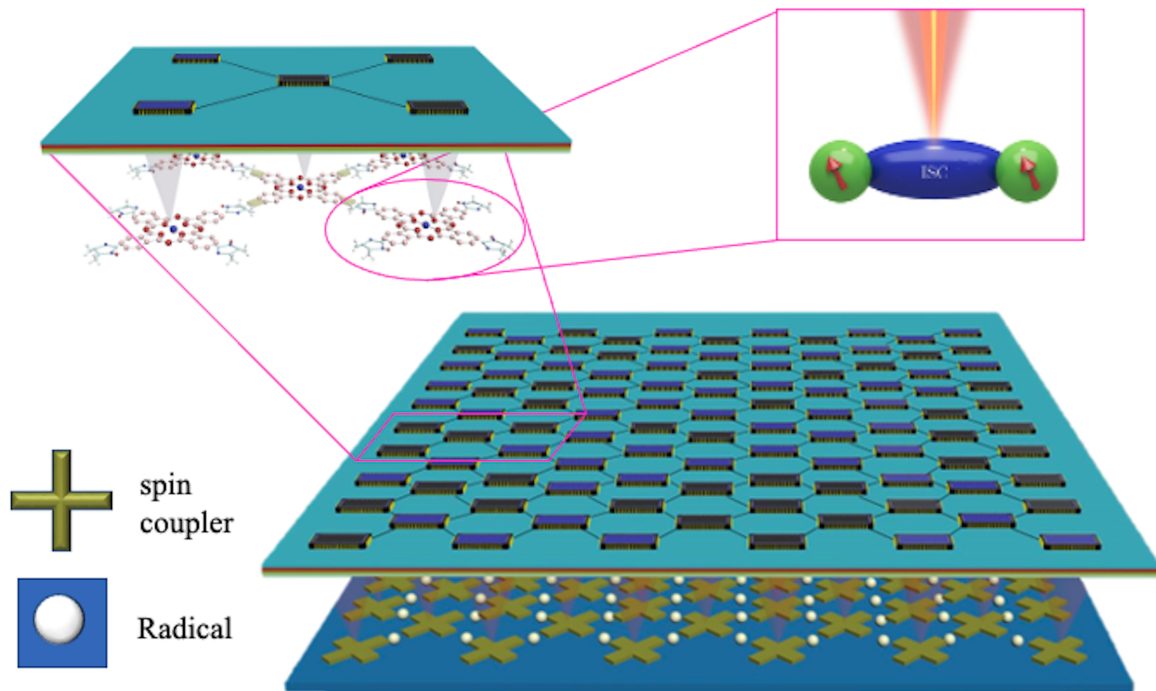


FIG. 4: (Color online.) A proposed QC architecture based on molecules and optical instruments is shown as an illustration for a more complex molecular QC network. The fundamental physical mechanism is through the optical excitation and ISC, linking the radicals, as computed in the previous sections in the paper. Here radicals (TYY as examples) are linked by the spin couplers (phthalocyanine molecules as examples), which could be either achieved by Van der Waals forces or through chemical bonds by designing bridging molecular structures. And the optical devices working as the control unit need to be fabricated close to the molecular spin couplers, such that we can program them as needed for a quantum gate operation [3].

iments. Our methodology presented here implies a universal route to design QC networks based on 2D OMNs by integrating optical instruments, spin coupler, and radical molecules. The related parameters such as light intensities, excitation wavelengths, and induced exchange interactions would be the key to facilitate the choice of suitable molecules for such QC design. The blueprint proposed here will not only scale up the QC networks by orders of magnitude compared with the current one based on superconducting qubits, but also have a great

potential to work at much higher temperature.

Data Availability

All the computer code and data that support the findings of this study are available from the corresponding author upon reasonable request.

-
- [1] Y. Alexeev, et al. Quantum computer systems for scientific discovery. *PRX Quantum* **2**, 017001 (2021).
 - [2] R. Thew, et al. Focus on quantum science and technology initiatives around the world. *Quantum Sci. Technol.* **5**, 010201 (2020).
 - [3] F. Arute, et al. Quantum supremacy using a programmable superconducting processor. *Nature* **574**, 505-510 (2019).
 - [4] Y. Wu, et al. Strong quantum computational advantage using a superconducting quantum processor. *Phys. Rev. Lett.* **127**, 180501 (2021).
 - [5] S. Ebadi, et al. Quantum phases of matter on a 256-atom programmable quantum simulator. *Nature* **595**, 227-232 (2021).
 - [6] W. Huang, et al. Fidelity benchmarks for two-qubit gates in silicon. *Nature* **569**, 532-536 (2019).
 - [7] X. Xue, et al. CMOS-based cryogenic control of silicon quantum circuits. *Nature* **593**, 205-210 (2021).
 - [8] L. Ma, et al. Triplet-radical spin entanglement: potential of molecular materials for high-temperature quantum information processing. *NPG Asia Mater.* **14**, 45-54 (2022).
 - [9] S. L. Bayliss, et al. Optically addressable molecular spins for quantum information processing. *Science* **370**, 1309-1312 (2020).
 - [10] M. R. Wasielewski, et al. Exploiting chemistry and molecular systems for quantum information science. *Nat. Rev. Chem.* **4**, 490-504 (2020).
 - [11] M. Gibertini, et al. Magnetic 2D materials and het-

- erostuctures. *Nat. Nanotechnol.* **14**, 408-419 (2019).
- [12] M. Atzori, et al. The second quantum revolution: role and challenges of molecular chemistry. *J. Am. Chem. Soc.* **141**, 11339-11352 (2019).
 - [13] M. Kjaergaard, et al. Superconducting qubits: Current state of play. *Annu. Rev. Condens. Matter Phys.* **11**, 369-395 (2020).
 - [14] A. Gaita-Ariño, et al. Molecular spins for quantum computation. *Nat. Commun.* **11**, 301-309 (2019).
 - [15] M. Atzori, et al. Room-temperature quantum coherence and rabi oscillations in vanadyl phthalocyanine: toward multifunctional molecular spin qubits. *J. Am. Chem. Soc.* **138**, 2154-2157 (2016).
 - [16] A. Auffèves. Quantum technologies need a quantum energy initiative. *PRX Quantum* **3**, 020101 (2022).
 - [17] M. A. Nielsen, et al. *Quantum computation and quantum information* (Cambridge Univ. Press, 2000).
 - [18] M. Warner, et al. Potential for spin-based information processing in a thin-film molecular semiconductor. *Nature* **503**, 504-508 (2013).
 - [19] A. M. Stoneham, et al. Optically driven silicon-based quantum gates with potential for high-temperature operation. *J. Phys. Condens. Matter* **15**, 447-451 (2003).
 - [20] R. D. Delaney, et al. Superconducting-qubit readout via low-backaction electro-optic transduction. *Nature* **606**, 489-493 (2022).
 - [21] O. Sato, et al. Control of magnetic properties through external stimuli. *Angew. Chem. Int. Ed.* **46**, 2152-2187 (2007).
 - [22] X. Zhang, et al. Electron spin resonance of single iron phthalocyanine molecules and role of their non-localized spins in magnetic interactions. *Nat. Chem.* **14**, 59-65 (2022).
 - [23] D. Dolphin. *The porphyrins* (Academic Press, 1979).
 - [24] K. Ishii, et al. Phthalocyanine-based fluorescence probes for detecting ascorbic acid: phthalocyaninatosilicon covalently linked to TEMPO radicals. *ChemComm* **47** 4932-4934 (2011).
 - [25] C. Corvaja, et al. CIDEP of fullerene C₆₀ biradical bisadducts by intramolecular triplet-triplet quenching: a novel spin polarization mechanism for biradicals. *Chem. Phys. Lett.* **330**, 287-292 (2000).
 - [26] Y. Teki, et al. Intramolecular spin alignment utilizing the excited molecular field between the triplet ($S = 1$) excited state and the dangling stable radicals ($S = 1/2$) as studied by time-resolved electron spin resonance: observation of the excited quartet ($S = 3/2$) and quintet ($S = 2$) states on the purely organic π -conjugated spin systems. *J. Am. Chem. Soc.* **122** 984-985 (2000).
 - [27] Y. Teki, et al. Excited high spin states of novel π -conjugated verdazyl radicals: photoinduced spin alignment utilizing the excited molecular field. *Mole. Phys.* **100** 1385-1394 (2002).
 - [28] L. Franco, et al. TR-EPR of single and double spin labelled C₆₀ derivatives: observation of quartet and quintet excited states in solution. *Mole. Phys.* **104** 1543-1550 (2006).
 - [29] A. C. Ferrari, et al. Science and technology roadmap for graphene, related two-dimensional crystals, and hybrid systems. *Nanoscale* **7**, 4598-4810 (2015).
 - [30] X. Zhuang, et al. Two-dimensional soft nanomaterials: a fascinating world of materials. *Adv. Mater.* **27**, 403-427 (2015).
 - [31] P. Huai, et al. Electronic control of spin alignment in π -conjugated molecular magnets. *Phys. Rev. B* **72**, 094413 (2005).
 - [32] H-P. Breuer, et al. *The theory of open quantum systems* (Oxford Univ. Press on Demand, 2002).
 - [33] M. J. Frisch, et al. Gaussian 03 (Gaussian, Inc., Pittsburgh, PA, 1998).
 - [34] W. Wu, et al. Electronic structure and exchange interactions in cobalt-phthalocyanine chains. *Phys. Rev. B* **88**, 024426 (2013).
 - [35] A. D. Becke. Density-functional thermochemistry. III. The role of exact exchange. *J. Chem. Phys.* **98**, 5648-5652 (1993).
 - [36] W. Wu. Hybrid-exchange density-functional theory study of the electronic structure of MnV₂O₄: Exotic orbital ordering in the cubic structure. *Phys. Rev. B* **91**, 195108 (2015).
 - [37] T. Zou, et al. Crystal structure tuning in organic nanomaterials for fast response and high sensitivity visible-NIR photo-detector. *J. Mater. Chem. C* **6**, 1495-1503 (2018).
 - [38] V. Ivády. Longitudinal spin relaxation model applied to point-defect qubit systems. *Phys. Rev. B* **101**, 155203 (2020).
 - [39] A. Blank, et al. Triplet line shape simulation in continuous wave electron paramagnetic resonance experiments. *Concepts Magn. Reson. A* **25**, 18-39 (2005).
 - [40] S. K. Misra, et al. Multifrequency electron paramagnetic resonance: theory and applications (John Wiley & Sons, 2011).
 - [41] H. Noda, et al. Critical role of intermediate electronic states for spin-flip processes in charge-transfer-type organic molecules with multiple donors and acceptors. *Nat. Mater.* **18**, 1084-1090 (2019).
 - [42] A. A. Ovchinnikov. Multiplicity of the ground state of large alternant organic molecules with conjugated bonds. *Theor. Chim. Acta* **47**, 297-304 (1978).
 - [43] E. H. Lieb. Two theorems on the Hubbard model. *Phys. Rev. Lett.* **62**, 1201-1204 (1989).
 - [44] P. W. Anderson. New approach to the theory of superexchange interactions. *Phys. Rev.* **115**, 2-13 (1959).
 - [45] A. T. Boothroyd. *Principles of Neutron Scattering from Condensed Matter* (Oxford Univ. Press 2020).
 - [46] X. Gao, et al. Quantum computer aided design simulation and optimization of semiconductor quantum dots. *J. App. Phys.* **114**, 164302 (2013).
 - [47] Y. M. Niquet, et al. Challenges and perspectives in the modeling of spin qubits. *IEEE International Electron Devices Meeting (IEDM)* **20**, 653-656 (2020).
 - [48] T. H. Kyaw, et al. Quantum computer-aided design: digital quantum simulation of quantum processors. *Phys. Rev. Appl.* **16**, 044042 (2021).
 - [49] T. Đorđević, et al. Entanglement transport and a nanophotonic interface for atoms in optical tweezers. *Science* **373**, 1511-1514 (2021).
 - [50] J. Kern, et al. Nanoscale positioning of single-photon emitters in atomically thin WSe₂. *Adv. Mater.* **28**, 7101-7105 (2016).
 - [51] J. Ziegler, et al. Single-photon emitters in boron nitride nanococoons. *Nano Lett.* **18**, 2683-2688 (2018).
 - [52] L. Peng, et al. Creation of single-photon emitters in WSe₂ monolayers using nanometer-sized gold tips. *Nano Lett.* **20**, 5866-5872 (2020).
 - [53] M. R. Rosenberger, et al. Quantum calligraphy: writing single-photon emitters in a two-dimensional materials

- platform. *ACS Nano* **13**, 904–912 (2019).
- [54] S. Liu, et al. Nanoscale positioning approaches for integrating single solid-state quantum emitters with photonic nanostructures. *Laser Photonics Rev.* **15**, 2100223 (2021).
- [55] C. Toninelli, et al. Single organic molecules for photonic quantum technologies. *Nat. Mater.* **20**, 1615–1628 (2021).
- [56] S. C. Benjamin, et al. Quantum computing with an always-on heisenberg interaction. *Phys. Rev. Lett.* **90**, 247901 (2003).

Acknowledgments

The authors gratefully acknowledge Prof. Hao Gong (National University of Singapore), Prof. Jing Liu (Technical Institute of Physics and Chemistry, CAS & Tsinghua University), Prof. Andrew Fisher, Prof. Gabriel Aeppli, Prof. Sandrine Heutz, Prof. Chris Kay, Dr. Garvin Morley, the late Prof. Marshall Stoneham, and Dr. Marc Warner, for helpful discussions. The authors thank the National Natural Science Foundation of China

(Nos. 62164006 and 11564023), Yunnan Fundamental Research Projects (No. 202101AS070036), Yunnan Local University Joint Special Funds for Basic Research (Nos. 2017FH001-007 and 2018FH001-017), Scientific Research Fund of Yunnan Education Department (Nos. 2020Y0464, 2021Y704, and 2021Y713), UK Research Councils Basic Technology Program (EP/F041349/1), and EU Marketplace Project 545083 for funding.

AUTHOR CONTRIBUTIONS

W. W., T. Y. Z, and H. W. contributed to the concept of the paper. J. W. C., T. H. H., L. M. and W. W. performed the theoretical analysis. All the authors contributed to the drafting of the paper.

Competing Interests

The authors declare no competing interests.